



A generic analytical solution for modelling pumping tests in wells

Benoît Dewandel, Sandra Lanini, Patrick Lachassagne, Jean-Christophe Maréchal

► To cite this version:

Benoît Dewandel, Sandra Lanini, Patrick Lachassagne, Jean-Christophe Maréchal. A generic analytical solution for modelling pumping tests in wells. *Journal of Hydrology*, 2018, 559, pp.89 - 99. 10.1016/j.jhydrol.2018.02.013 . hal-01814503

HAL Id: hal-01814503

<https://brgm.hal.science/hal-01814503>

Submitted on 13 Jun 2018

HAL is a multi-disciplinary open access archive for the deposit and dissemination of scientific research documents, whether they are published or not. The documents may come from teaching and research institutions in France or abroad, or from public or private research centers.

L'archive ouverte pluridisciplinaire **HAL**, est destinée au dépôt et à la diffusion de documents scientifiques de niveau recherche, publiés ou non, émanant des établissements d'enseignement et de recherche français ou étrangers, des laboratoires publics ou privés.

A generic analytical solution for modelling pumping tests in wells intersecting fractures

Benoît Dewandel^{*a}, Sandra Lanini^a, Patrick Lachassagne^b and Jean-Christophe Maréchal^a

^a BRGM, D3E/NRE-University of Montpellier, 1039 rue de Pinville, 34000 Montpellier, France. b.dewandel@brgm.fr; s.lanini@brgm.fr; jc.marechal@brgm.fr

^b Water Institute by Evian, Evian-Volvic-World, Danone Waters, Evian-les-Bains, France. patrick.lachassagne@danone.com

^{*} Corresponding author

Abstract

The behaviour of transient flow due to pumping in fractured rocks has been studied for at least the past 80 years. Analytical solutions were proposed for solving the issue of a well intersecting and pumping from one vertical, horizontal or inclined fracture in homogeneous aquifers, but their domain of application—even if covering various fracture geometries—was restricted to isotropic or anisotropic aquifers, whose potential boundaries had to be parallel or orthogonal to the fracture direction. The issue thus remains unsolved for many field cases. For example, a well intersecting and pumping a fracture in a multilayer or a dual-porosity aquifer, where intersected fractures are not necessarily parallel or orthogonal to aquifer boundaries, where several fractures with various orientations intersect the well, or the effect of pumping not only in fractures, but also in the aquifer through the screened interval of the well.

Using a mathematical demonstration, we show that integrating the well-known Theis analytical solution (Theis, 1935) along the fracture axis is identical to the equally well-known analytical solution of Gringarten et al. (1974) for a uniform-flux fracture fully penetrating a homogeneous aquifer. This result implies that any existing line- or point-source solution can be used for implementing one or more discrete fractures that are intersected by the well. Several theoretical examples are presented and discussed: a single vertical fracture in a dual-porosity aquifer or in a multi-layer system (with a partially intersecting fracture); one and two inclined fractures in a leaky-aquifer system with pumping either only from the fracture(s), or also from the aquifer between fracture(s) in the screened interval of the well. For the cases

with several pumping sources, analytical solutions of flowrate contribution from each individual source (fractures and well) are presented, and the drawdown behaviour according to the length of the pumped screened interval of the well is discussed. Other advantages of this proposed generic analytical solution are also given.

The application of this solution to field data should provide additional field information on fracture geometry, as well as identifying the connectivity between the pumped fractures and other aquifers.

To protect this original concept of a generic solution for modelling pumping tests in fractured media, a patent application has been deposited on parts of this work (French National Institute of Industrial Property).

Key words: analytical solution, pumping in discrete fractures, fractured rocks, pumping test

1. Introduction

Since the late 1930s (e.g., Strelsova, 1988), much work has been carried out to characterize the transient flow of pumping tests carried out in naturally or artificially fractured aquifers (e.g. Muskat, 1937; Warren and Root, 1963; Russell and Truitt, 1964; Bertrand et al., 1980; Barker, 1988; Moench, 1984; Hamm and Bidaux, 1996; Jourde et al., 2002; Tiab, 2005; Delay et al., 2007; Rafini and Larocque, 2012; Dewandel et al., 2014; Roques et al., 2016). This led to the development of several analytical solutions for understanding the flow behaviour created by a well intersecting and pumping one vertical, horizontal or inclined fracture with infinite or finite hydraulic conductivity embedded in a homogeneous aquifer (Gringarten and Ramey, 1973, 1974; Gringarten et al., 1974; Cinco-Ley et al., 1975, 1998, Thiery, 1980; see also the PetroWiki website). These solutions were obtained by applying the Green's and source functions and the Newman's product method (Newman, 1936; Gringarten and Ramey, 1974). However, their domain of application, though proposed for a variety of fracture geometries, is restricted to isotropic or anisotropic infinite aquifers that may be limited in space by no-flow or constant-head boundaries (Gringarten et al., 1974), leaving several possibilities unsolved. For example, pumping a fracture in a multilayer or dual-porosity aquifer, where the fracture is not necessarily parallel or orthogonal to the aquifer boundaries, or a well intersecting and pumping fractures with various orientations, or the effect of

pumping from both fractures and also the aquifer in front of the screened interval of the well, etc.

The aim of our research was to seek a new and alternative solution for computing drawdown while pumping in one or several fractures, based on existing line or point source solutions. We first demonstrate that the solutions developed for pumping in a vertical fracture can directly be found by integrating the Theis analytical solution (Theis, 1935) along the fracture axis. Then, by extension, line-source solutions for dual-porosity and multi-layer aquifers and a point-source solution for a leaky aquifer are used when pumping discrete fractures in such aquifers. Theoretical examples are given for pumping in: *i*) A fracture in a dual-porosity aquifer; *ii*) A fracture in a multi-layer system that fully or partially intersects one of the aquifer layers; *iii*) An inclined fracture in a homogeneous aquifer; *iv*) Two inclined fractures in a leaky-aquifer system with pumping only in the fractures (i.e. the well is only screened in front of the fractures); and *v*) The same as *iv*), but now pumping in both the fractures and the aquifer through the well itself (screened interval). As in *iv*) and *v*), the flowrate contributions of each pumped source (i.e., the two fractures and the screened interval of well) to the total pumping rate vary over time, analytical solutions for evaluating their relative contributions are also presented.

We do not suggest that the proposed solution should replace existing models used for modelling drawdown in pumping tests performed in homogeneously fractured media (e.g., Barker, 1988; Moench, 1984; Hamm and Bidaux, 1996), or for pumping in fractures in homogeneous aquifers (e.g., Gringarten et al, 1974; Thiéry, 1980). Rather, they are meant to supplement existing models by providing additional hydrogeological information.

2. Mathematical demonstration

Here, we demonstrate that the well-known Theis analytical solution (1935), defined for a well fully penetrating an isotropic aquifer and integrated along a fracture axis, is strictly identical to the analytical solution of pumping in one vertical fracture proposed by Gringarten et al. (1974), with uniform flux distribution along the fracture plane. In this conceptual aquifer model (Fig. 1), the well intercepts the middle of a vertical fracture of length $2x_f$ and negligible thickness, intersecting a homogeneous and infinite aquifer of transmissivity T and storage

coefficient S . Hereafter, we briefly show how we achieved this demonstration; more details can be found in the *Supplemental Materials*.

Assuming that the conductivity of the fracture can be considered infinite, and integrating the Theis well function along the fracture plane leads to the following equation:

$$s_I(x, y, t) = \frac{1}{4\pi T} \int_{-x_f}^{+x_f} q(x) E_1 \left(\underbrace{\frac{(x - x_{obs})^2 + y_{obs}^2}{4Tt} S}_{\text{Theis well function}} \right) dx \quad \text{Eq.1}$$

Theis well function

where $q(x)$ is the rate of pumping per unit length of the fracture, t the time since starting the pumping, and E_1 the exponential integral (see Fig. 1 for parameters that are not defined in the text). Assuming that the pumping rate Q is uniformly distributed along the fracture, then $q(x)$ takes the following form:

$$Q = \int_{-x_f}^{+x_f} q(x) dx \Rightarrow q(x) = q = \frac{Q}{2x_f} \quad \text{Eq.2}$$

Using this statement and the following dimensionless variables: $t_D = \frac{Tt}{x_f^2 S}$; $x_D = \frac{x_{obs}}{x_f}$;

$y_D = \frac{y_{obs}}{x_f}$, Eq.1 becomes:

$$s_I(x, y, t) = \frac{Q}{2\pi T} \frac{1}{4x_f} \int_{-x_f}^{+x_f} \left(\int_0^{t_D} \frac{e^{-\left[\left(\frac{x}{x_f} - x_D\right)^2 + y_D^2\right]/4\tau}}{\tau} d\tau \right) dx \quad \text{Eq.3}$$

According to the Fubini theorem (τ and x being independent variables), the order of the integration can be inverted, and as $e^{-y_D^2/4\tau}$ does not depend on x , Eq.3 can be rearranged as:

$$s_I(x, y, t) = \frac{Q}{2\pi T} \frac{1}{x_f} \int_0^{t_D} e^{-y_D^2/4\tau} \underbrace{\left(\int_{-x_f}^{+x_f} \frac{e^{-\left(\frac{x}{x_f} - x_D\right)^2/4\tau}}{4\tau} dx \right)}_{(a)} d\tau \quad \text{Eq.4}$$

(a)

108 When changing variable $v = \left(\frac{x}{x_f} - x_D \right) / 2\sqrt{\tau}$, the term (a) can be separated into two terms
 109 related to the *Erf* function, such as:

$$110 \quad a = \int_{-x_f}^{+x_f} \frac{e^{-\left(\frac{x}{x_f} - x_D\right)^2 / 4\tau}}{4\tau} dx = \frac{x_f \cdot \sqrt{\pi}}{4\sqrt{\tau}} \left[-\operatorname{Erf}\left(\frac{(1+x_D)}{2\sqrt{\tau}}\right) + \operatorname{Erf}\left(\frac{(1-x_D)}{2\sqrt{\tau}}\right) \right] \quad \text{Eq.5}$$

111 Combining Eq.4 and Eq.5, we obtain:

$$112 \quad s_I(x, y, t) = \frac{Q}{2\pi T} \int_0^{t_D} e^{-\frac{y_D^2}{4\tau}} \left[\operatorname{Erf}\left(\frac{1-x_D}{2\sqrt{\tau}}\right) - \operatorname{Erf}\left(\frac{1+x_D}{2\sqrt{\tau}}\right) \right] \frac{\sqrt{\pi}}{4\sqrt{\tau}} d\tau \quad \text{Eq.6}$$

113 Eq.6 demonstrates that the Theis analytical solution, when integrated along the fracture axis,
 114 corresponds exactly to the Gringarten et al. (1974) analytical solution (their Eq.20) using
 115 Green's and source functions and the Newman's product method for a vertical fracture with
 116 an uniform flux distribution that fully penetrates the aquifer.

117 This implies that the integration of any line-source solution (i.e. a well function defined for a
 118 fully or partially penetrating well) along the fracture axis can be used for computing
 119 drawdown caused by pumping from a vertical fracture that partially or fully penetrates the
 120 aquifer. In addition, any point-source solution can be used for computing drawdown while
 121 pumping an inclined or a vertical fracture that is intersected by a well.

122

123 **3. Theoretical examples**

124 This section presents theoretical examples based on the integration of known analytical line-
 125 or point-source solutions along the fracture plane. They are based on equation Eq.1 from
 126 which the inner integral (Theis well function in Eq.1) is replaced by another well function,
 127 assuming that flux is uniformly distributed along the fracture (Eq.2). Dimensionless
 128 drawdown (s_D) and its logarithmic derivative (s_D') vs. dimensionless time with respect to
 129 fracture length (t_{Dxf} or t_{DL} , see appendix A) were computed for creating Log-Log diagnostic
 130 plots and examining transient flow regimes (Bourdet et al., 1983; Deruyck et al., 1992;
 131 Renard et al., 2009; Rafini et al., 2017, etc.). As benchmarks, the solutions were compared to
 132 existing analytical solutions for pumping in a vertical and a horizontal fracture in a
 133 homogeneous aquifer (Gringarten et al., 1974; Thiéry, 1980).

3.1 Vertical fractures

These analytical solutions are found by integrating line-source solutions. Because the analytical integration of a given line-source solution along the fracture can be too difficult, we approximate it by first dividing the fracture length into smaller segments and then placing a line-source solution at each segment. Because of the linear properties of the diffusivity equation, we used the principle of superposition, summing up drawdowns induced by each segment to provide the total drawdown value due to pumping in the fracture. Then, this general formulation is used for integrating the solutions numerically:

$$s_{w-f}(x, y, t, x_f, \lambda, \alpha, \dots) = \frac{Q}{4\pi T \cdot M} \sum_{i=1,2,3..}^M s_w(x_i, y, t, \lambda, \alpha, \dots) \quad \text{Eq.7}$$

where $s_w(x, y, t, \lambda, \alpha, \dots)$ is a known line-source solution (e.g. dual-porosity, dual-permeability or partially penetrating well solutions) and $s_{w-f}(x_i, y, t, x_f, \lambda, \alpha, \dots)$ is the solution for pumping from a vertical fracture with half-length x_f (Fig. 1) in an aquifer whose parameters are defined in the s_w solution (λ, α, \dots). The fracture is along the x -axis, M is the number of segments, and x_i is the abscissa of the middle of each segment ($-x_f \leq x_i \leq +x_f$).

3.1.1. Pumping at the centre of a vertical fracture fully penetrating a dual-porosity medium

Figure 2 provides an example of the use of Eq.7 with Moench's (1984) dual-porosity model (a model frequently used for interpreting pumping tests performed in homogeneously fractured media). Here, the implemented fracture is vertical and fully penetrates the dual-porosity aquifer (e.g. Fig. 1). Figure 2 shows how pumping in a fracture behaves for a set of interporosity flow coefficients λ (see caption for explanation of λ). As expected, when $\lambda=0$ (i.e. the matrix hydraulic conductivity is nil corresponding to a single-porosity aquifer), the solution is equivalent to the Gringarten et al. (1974) analytical solution, with an error of 0.2% ($error = |s_G - s_{w-f}| / s_G$, s_G being Gringarten's solution; Eq.6). The difference between the theoretical solution and its numerical evaluation shows that discretization (division of the fracture length into smaller elements) errors are very small.

At the start of pumping, as expected, the flow is linear (half-unit slope of derivative curves) and corresponds to flow from the most permeable medium (i.e. the secondary porosity) to the vertical fracture. For intermediate pumping stages, the derivative curves have a classical 'U'

shape, characterizing the flow from primary (the block matrix) to secondary porosity of the dual-porosity aquifer. Then, for late pumping stages, the derivatives form a plateau that corresponds to radial flow from the dual-porosity aquifer to the vertical fracture ($s_D'=0.5$). In experimental data, this implies that drawdown values on a semi-logarithmic plot form a straight line from which the aquifer transmissivity can be deduced.

3.1.2. *Pumping at the centre of a vertical fracture partially penetrating the deepest layer of a multi-layer aquifer*

Our second example (Fig. 3a) corresponds to a multilayer aquifer, where pumping from the deepest aquifer induces depletion in the upper one. This system is characterized by a lower aquifer of thickness B with transmissivity T and storage coefficient S , and an upper aquifer with transmissivity T_0 , and storage coefficient S_y . Both aquifers are separated by an aquitard of hydraulic conductivity k' and thickness B' . The vertical fracture is located in the deeper aquifer and is characterized by its location in the aquifer (z_f = vertical coordinate of the fracture centre), its height h_f and its length $2x_f$. The line-source solution for this conceptual model is an extension of the Hunt and Scott (2007) model for a partially penetrating well.

Figure 3b shows type curves for various degrees of penetration of the fracture into the aquifer (h_f/B ratio). In these examples, the fracture is located at the centre of the deepest aquifer ($z_f/B=0.5$), and there is no hydraulic conductivity anisotropy ($k_x=k_y=k_z$). As expected when h_f equals aquifer thickness (B), the solution is identical to the Gringarten et al. (1974) analytical solution until leakage from the upper aquifers starts. At the start of pumping, derivative curves follow the half-unit slope that shows linear flow from the aquifer to the fracture, before decreasing and following a negative slope tending to $-1/2$ that corresponds to ellipsoidal flow because of the partial entry of the fracture into the aquifer (low h_f/B ratios, curve 5 in Fig. 3b for instance). For intermediate times, the derivative curves form a first plateau corresponding to radial flow into the lower pumped aquifer ($s_D'=0.5$). Later, they have a 'V' shape characterizing leakage from the upper aquifers. Finally, for very late stages of pumping, derivative curves form a second plateau whose value depends on the transmissivity values of both upper and lower aquifers ($s_D'=T/2(T+T_0)$).

3.2 Inclined fractures

3.2.1 *Pumping at the centre of a single inclined fracture*

Figure 4a presents the conceptual model. The aquifer is characterized by transmissivity T and a storage coefficient S , and is anisotropic (k_x , k_y , k_z). It is overlain by a leaky aquifer of thickness B' and hydraulic conductivity k' . This conceptual aquifer model is similar to that proposed by Hantush (1961) and assumes that the aquitard does not react to pumping (infinite storage). The fracture crosscuts the aquifer, and is characterized by length L , width l , and angle θ with the vertical axis. The analytical solution of drawdown for pumping in a fracture in such an aquifer is found by integrating the point-source analytical solution given by Hunt (2005) on the fracture plane:

$$s(x, y, z, t) = \frac{1}{2\pi T} \int_{-L/2}^{L/2} \int_{-l/2}^{l/2} q(\xi, \vartheta) \sum_{n=1}^{\infty} \frac{\cos(\alpha_n \xi) \cos(\alpha_n z/B)}{1 + \frac{\sin(2\alpha_n)}{2\alpha_n}} W\left(\frac{(r/B)^2}{4t_D}, \alpha_n \frac{r}{B} \sqrt{k_z/k_{xy}}\right) d\xi d\vartheta \quad \text{Eq.8}$$

where r is the radial distance to the well, B is aquifer thickness, k_z/k_{xy} its vertical anisotropy in hydraulic conductivity, t_D a dimensionless time, $q(\xi, \vartheta)$ the pumping rate per unit area, α_n the root of an equation, and $W(a, b)$ the Hantush leaky-aquifer well function; all parameters are explained in Appendix B.

As before, this equation is solved numerically by dividing the fracture in small elements along both L and l while assuming a uniformly distributed pumping rate per unit area (similarly to Eq.2; i.e. $q(\xi, \vartheta) = Q/(lL)$). Then the principle of superposition is applied for computing the drawdown at any location into the aquifer. Therefore, the solution yields:

$$s(x, y, z, t) = \frac{Q}{2\pi T \cdot M \cdot p} \sum_{j=1}^p \sum_{i=1}^M \sum_{n=1}^{\infty} \frac{\cos(\alpha_n z_{i,j}/B) \cos(\alpha_n z/B)}{1 + \frac{\sin(2\alpha_n)}{2\alpha_n}} W\left(\frac{(r_{i,j}/B)^2}{4t_D}, \alpha_n \frac{r_{i,j}}{B} \sqrt{k_z/k_{xy}}\right) \quad \text{Eq.9}$$

where $r_{i,j}$ is the radial distance between the point (x, y, z) and the i, j^{th} element, and M and p are the number of segments along L and l .

Figure 4b presents type curves of Eq.9 for various values of θ . For this example, the aquifer has a vertical anisotropy of 10.0 ($k_{xy}/k_z=10$) and we ignore the leaky aquifer ($k'/B'=0$). The fracture is located at the centre of the aquifer ($z_f/B=0.5$) and its width equals the aquifer thickness ($l=B$).

As expected, the results show that Eq.9 is identical to the benchmark solutions: the Gringarten et al. (1974) solution for a vertical rectangular fracture when $\theta=0^\circ$, and the Thiéry (1980)

solution for a horizontal rectangular fracture located at the centre ($z_f/B=0.5$) of the aquifer, when $\theta=90^\circ$. Derivative curves show that, regardless of the θ value, the early stages of pumping always describe linear flow within the fracture (half-unit slope of derivative curves). Later, derivatives create a hump, more or less pronounced according to the value of θ . This behaviour corresponds to the transition from flow perpendicular to the fracture—controlled by the average hydraulic conductivity normal to the fracture plane—to horizontal flow controlled by the horizontal aquifer transmissivity. In some cases (e.g. $\theta=90^\circ$), the derivatives follow a near-negative half-unit slope characterizing ellipsoidal flow because of the partial penetration of the fracture into the aquifer. Note also that increasing the k_{xy}/k_z ratio with $\theta \rightarrow 90$, will result in a more pronounced hump of the derivative curve, because of the increased resistance to flow induced by the low vertical hydraulic conductivity. When the fracture is vertical and fully penetrates the aquifer ($\theta=0^\circ$), the hump disappears as the drawdown no longer depends upon the vertical anisotropy in hydraulic conductivity. For the late stages of pumping, derivatives form a plateau characterizing the radial flow induced by flow towards the fracture at the aquifer scale ($s_D'=0.5$). As mentioned before, in experimental data the plateau value will depend on the horizontal transmissivity of the aquifer.

3.2.2 Pumping intersecting two fractures – Pumping in the fractures only

One of the flexibilities inherent in our analytical/numerical solution is the possibility to consider several fractures with different locations and orientations intersecting the pumping well. Figures 5 and 6 show an example of application where two fractures intersect the well. The characteristics of fracture 1 are L : 10 m; l : 20 m, θ : 20° , and z_f : 13 m, and of fracture 2 L : 10 m; l : 45 m, θ : 100° , and z_f : 5 m. As before, only fractures are pumped (uniform flux).

As shown previously, fractures with different orientations and locations are characterized by different flow behaviours. Consequently, their resistance to flow is different; this implies, when several fractures are pumped simultaneously, that the flowrates from each fracture vary over time. Therefore, the flowrate contributions of each fracture to the total pumping rate of the well have to be considered before evaluating the average drawdown in the well. To solve this problem, we again use the principle of superposition, i.e. the drawdown in a particular location is the sum of drawdown values of several pumping sources. This allows computing the flowrates of each fracture from the combination of dimensionless pumping-source solutions (see similar work in Lolon et al. 2008 and Lashgari et al., 2014). However, the boundary conditions of each individual solution do not include perturbation due to the

presence of the other pumping source, which is the only approximation of this solution. Note that this approximation is the same as the one used for modelling drawdown (with analytical solutions) created by several pumping wells.

As the well is screened in front of each fracture only and as it intersects the fracture centre, the average dimensionless drawdown in the well, s_{Dtot} , can be derived from the following equations:

$$s_{Dtot}Q = \frac{1}{2}[q_1(s_{D1} + s_{D12}) + q_2(s_{D2} + s_{D21})] \quad \text{Eq.10a}$$

$$Q = q_1 + q_2 \quad \text{Eq.10b}$$

where q_1 and q_2 are flowrates from fractures 1 and 2, Q is the total pumping flowrate. s_{D1} and s_{D2} are the dimensionless drawdown values at the centre of fractures 1 and 2, s_{D12} is the dimensionless drawdown induced by fracture 1 at the centre of fracture 2, and s_{D21} , the one induced by fracture 2 at the centre of fracture 1.

At the intersection between fracture 1 and the well, the drawdown is:

$$S_{F1} = q_1 s_{D1} + q_2 s_{D21} \quad \text{Eq.10c}$$

and at the intersection between fracture 2 and the well:

$$S_{F2} = q_2 s_{D2} + q_1 s_{D12} \quad \text{Eq.10d}$$

Assuming equal drawdown at the centre of both fractures ($S_{F1}=S_{F2}$), thus implicitly assuming uniform drawdown at the well location, and solving the system of equations provided by Eqs. 10, one will find solutions for s_{Dtot} , q_1 and q_2 :

$$s_{Dtot} = \frac{1}{2}(A + BC)/(1 + C) \quad \text{Eq.11a}$$

$$q_1 = Q/(1 + C), \text{ or } q_{D1} = 1/(1 + C) \quad \text{Eq.11b}$$

$$q_2 = QC/(1 + C), \text{ or } q_{D2} = C/(1 + C) \quad \text{Eq.11c}$$

with $A = (s_{D1} + s_{D12})$, $B = (s_{D2} + s_{D21})$ and $C = (s_{D1} - s_{D12})/(s_{D2} - s_{D21})$, and dimensionless flowrate $q_{Di} = q_i/Q$.

For the computation, drawdown values s_{D1} , s_{D2} , s_{D12} and s_{D21} were calculated separately with Eq.9 while assuming a unit flow rate ($Q=1$).

Figures 6a and b present the resulting drawdown and the flowrate contributions of each fracture, and figures 6c, d, e and f show drawdown distribution in the vertical plane at different times. In the early stages of pumping, the drawdown derivative is characterized by the classical half-unit slope corresponding to flow from the aquifer to both fractures ($t < 0.8$ min; Fig. 6a and c). In the beginning, both fractures contribute almost equally to the total pumping rate (Fig. 6b), though in the very early stage ($t \leq 0.1$ min) fracture 2 contributes slightly more because of its larger area. However, very rapidly flowrate from fracture 1 becomes dominant as its orientation offers less restriction to flow compared to fracture 2, which is oriented almost orthogonal to the hydraulic conductivity axis of the lower aquifer. Between 0.1 and 100 min, the derivative curve shows transitional flow behaviour, followed by a near $-1/2$ slope ($100 < t < 2000$ min) that characterizes the ellipsoidal flow towards both fractures as drawdown starts to progress in the whole aquifer (Fig. 6d). Later ($2000 < t < 7000$ min), the derivative stabilizes, forming a plateau characterizing radial flow from the aquifer to both fractures (Fig. 6e) whose value depends on the aquifer transmissivity. For the last stages ($t > 7000$ min), the derivative decreases because of leakage from the top aquitard (Fig. 6f). At the end of pumping, fracture 1 (the smallest; 200 m^2) contributes 74% of the total flow rate while fracture 2, the largest (450 m^2), contributes only 26% (Fig. 6b).

As a final point, this drawdown curve shows the difficulty of identifying the contribution of more than one fracture on a diagnosis plot, as this looks similar to one of the cases presented in Fig. 4 until leakage appears. In this case, only drawdown observation on other wells in the aquifer and/or few data on the geometry of fractures can provide unequivocal information about these fractures.

3.2.3. *Pumping intersecting two fractures – pumping in the fractures and in the aquifer through the well itself*

This last case is similar to the sketch presented on Figure 5, but pumping affects both fractures as well as the aquifer directly through a screened portion of the well. The well intersects the centres of both fractures. As for the previous case, flowrate contributions of each individual pumping source (the two fractures and the well) have to be evaluated before computing the average dimensionless drawdown, s_{Dtot} , in the well:

$$s_{Dtot}Q = q_1s_{D1W} + q_2s_{D2W} + q_ws_w \quad \text{Eq.12a}$$

$$\text{with } Q = q_1 + q_2 + q_w \quad \text{Eq.12b}$$

where q_1 and q_2 are flowrates from fractures 1 and 2, q_w the flowrate from the aquifer through the well and Q the total pumping flowrate. s_{D1W} and s_{D2W} are the dimensionless drawdown values induced by fractures 1 and 2 in the screened well interval. s_{D1W} and s_{D2W} are the average drawdown values along the screened interval, computed by integrating the analytical solution (Eq.8) between the upper and lower limits of the pumped section. s_w is the dimensionless drawdown induced by pumping in the screened interval (Hunt's (2005) analytical solution).

At the intersection between fractures and the well, the drawdown in the well has to be identical to that from the fractures. Therefore, at the intersection between the well and fracture 1:

$$q_ws_w = q_1s_{D1} + q_2s_{D21} \quad \text{Eq.12c}$$

and between the well and fracture 2:

$$q_ws_w = q_2s_{D2} + q_1s_{D12} \quad \text{Eq.12d}$$

with s_{D1} and s_{D2} the dimensionless drawdown values at the centre of fractures 1 and 2, s_{D12} the dimensionless drawdown induced by fracture 1 at the centre of fracture 2, and s_{D21} the one induced by fracture 2 at the centre of fracture 1.

Assuming equal drawdown at the centre of both fractures (Eq.12c=Eq.12d) in the well in front of both fractures, and solving the system of equations provided by Eqs.12, solutions are found for s_{Dtot} , q_1 , q_2 and q_w :

$$s_{Dtot} = (s_{1W} + Cs_{2W} + D)/(1 + C + D/s_w) \quad \text{Eq.13a}$$

$$q_1 = Q/(1 + C + D/s_w), \text{ or } q_{D1} = 1/(1 + C + D/s_w) \quad \text{Eq.13b}$$

$$q_2 = QC/(1 + C + D/s_w), \text{ or } q_{D2} = C/(1 + C + D/s_w) \quad \text{Eq.13c}$$

$$q_w = QD/[s_w(1 + C + D/s_w)], \text{ or } q_{DW} = D/[s_w(1 + C + D/s_w)] \quad \text{Eq.13d}$$

where C is defined before (Eqs.11), $D = (s_{D1}s_{D2} - s_{D12}s_{D21}) / (s_{D2} - s_{D21})$, and $q_{Di} = q_i / Q$ are the dimensionless flowrates.

Drawdown computations and flowrate of each pumping source were made for a well fully penetrating an aquifer with characteristics and fractures as sketched on Figure 5. Drawdown values were computed separately with Eq.9 for the fractures and with the Hunt (2005) analytical solution for the well (vertical, fully penetrating the aquifer and uniform flux distribution). Figures 7a and b show the results and Figures 7c, d, e and f the drawdown distribution (on a vertical axis) at different times.

The drawdown behaviour is very different to the case where only the fractures are pumped (Fig. 6a). At the start of pumping (see also Fig. 7c), the half-unit slope persists as the contribution of the aquifer through the well in terms of flowrate is low compared to that from the fractures (Fig. 7b). After 1 to ~1000 minutes, the derivative curve slightly decreases, following a gentle near-negative slope. This period describes the transitional flow regime during which the contribution through the well starts to contribute significantly to the total flowrate. During this period, ellipsoidal flows from fractures still exist (Fig. 7d), but are masked by the well contribution. Between 1000 and ~7000 minutes (Fig. 7e), the derivative curve forms a plateau corresponding to near-radial flow induced by the three pumping sources. At the end of pumping, the well contributes up to 52% of the total flow rate, fracture 1 up to 36%, while fracture 2 yields only 12%.

The high flowrate contribution from the aquifer to the well, here equivalent to both fractures, is due to two reasons: *i*) The medium to high transmissivity of the aquifer ($T=10^{-4} \text{ m}^2/\text{s}$), or more exactly its diffusivity; and *ii*) Because the screened interval covers the entire aquifer thickness. If the aquifer transmissivity had been very low (e.g. $<10^{-8} \text{ m}^2/\text{s}$), or if the well had been screened near the fractures, the aquifer contribution through the well would have been negligible or drastically less, creating an average drawdown in the well similar to the one observed on Fig. 6. Appendix C provides an intermediate figure where the well is screened in front of both fractures only. Fractures and aquifer properties are those of Fig. 5 with a well-screened interval of 7 m. Drawdown and derivative behaviour are different from the previous case, and closer to those of Fig. 6 because of the lower contribution of the aquifer through the well to the total pumping flowrate (at the end of pumping, well: 20%, fracture1: 56% and fracture 2: 22%).

This result shows that where an aquifer has significant transmissivity, the fracture signature (i.e. the half-unit derivative slope in the early stages of pumping) may be very short, and even not seen. This may explain why pumping tests in fractured media commonly are not interpreted with solutions invoking discrete fractures intersected by the well, but with homogeneous aquifer solutions (e.g. dual-porosity models), even if fractures were seen on field data (e.g. Taylor and Howard, 2000; Maréchal et al., 2004; Dewandel et al., 2011, 2017).

4. Conclusions

Integrating the well-known Theis analytical solution (1935) along a fracture axis is mathematically identical to the equally well-known solution of Gringarten et al. (1974) for a uniform-flux fracture fully penetrating an aquifer, obtained with Green's function and the product solution method. Though this result was mathematically expected (Green's function represents the distribution of instantaneous point-sources over length, area or volume), this had never before been demonstrated or highlighted as far as we are aware. This implies that any line- or point-source solution integrated along the fracture plane can be used for computing flow through a fracture. In view of the large number of existing analytical solutions, this provides a very wide range of applications for this generic analytical solution, and thus helps modelling discrete fractures that are intersected and pumped by a well, in most hydrogeological settings.

We give several theoretical examples for dual-porosity or multilayer aquifer types, even when the pumping well intersects several fractures, and for pumping both in fractures and/or directly in the aquifer through the screened interval of a well. Where several sources are pumped (the aquifer through the well and/or several fractures), solutions of flowrate contributions of each individual pumping source are given and can be extended to any number of fractures.

As expected when the conceptual hydrogeological models respect the theoretical assumptions of benchmark analytical solutions (here for pumping in a vertical or a horizontal fracture), the proposed solutions do not show significant differences between models.

Where a fracture is vertical and fully intersects the aquifer, the classical flow regime of a fracture can be recognized regardless of the conceptual aquifer model used. However, in the case of an inclined fracture, we show that flow behaviour is not unique. In that case, it

depends on the screened-interval length of the well, as well as on whether only the fracture, or both the fracture and the surrounding aquifer are screened. Even, when aquifer transmissivity (or diffusivity) is not low, the fracture signature (the classical half-unit slope on a derivative drawdown curve) can be masked by the contribution of the screened interval of the well.

Our work is based on the assumption that flux is uniformly distributed along the fracture and the screened interval of the well. Even if this hypothesis is the closest approximation for an infinite conductivity fracture –it is nonetheless identical at early stages of pumping- solutions for infinite conductivity fracture can be derived from uniform flux analytical solutions (Gringarten et al., 1974). This can be computed by dividing the fracture into small sections, each with uniform flux per unit area, and then by evaluating the flow contribution of each section to arrive at identical drawdown values along the entire fracture, including the screened interval of the well if it is pumped as well.

In addition to the possibility of using any line- or point-source solutions, our generic analytical solution offers several other advantages. For example, by using the superposition principle (image well theory) it allows developing solutions where no-flow and constant-head boundaries are not necessarily parallel to the fracture directions. Currently available analytical solutions, however, assume fractures parallel or at right angle to boundaries. In the case of a well field, our solution allows computing the overall drawdown created by several pumping wells intersecting fractures with various geometries, or when only some of the wells intersect such fractures, the others directly pumping the aquifer. Finally, though we established analytical solutions for rectangular fractures, these solutions can also be developed for any other geometrical configuration.

From a practical point view, the proposed analytical solutions and few diagnosis plots as presented provide additional information on flow behaviour and drawdown in fractured media. Their application to real field data is expected soon to characterize fracture geometries, particularly in the case of fractured thermo-mineral aquifers (Maréchal et al., 2014). This should help defining, among other points, the location of a well within a given deep fracture, and then to establish if this fracture extends very deep or not. In addition, it should help characterizing fractures of the weathered Stratiform Fractured Layer of hard rock aquifers (Lachassagne et al., 2011) as well as their relationships with overlying saprolite (leakage effects).

Acknowledgements

This study was partly conducted under a research agreement between Evian-Volvic World (Water Institute by Evian, Danone Waters France) and BRGM. We are grateful to Dr. H.M. Kluijver for revising the English text.

References

- Barker, J.A., 1988. A generalized radial flow model for hydraulic tests in fractured rock, *Water Res. Res.*, 24, 1796-1804.
- Bertrand, L, Feuga, B., Noyer, M.L., Thiéry, D., 1980. Hot Dry Rocks, contribution to the methodology of determining the hydraulic properties of naturally or artificially fractured rocks. In French, BRGM report 80SGN029GEG, 229 p.
- Bourdet, D., Whittle, T.M., Dougals, A.A., Pirard, V.M., 1983. A new set of type curves simplifies well test analysis, *World Oil.*, May, 95-106.
- Cinco-Ley, H., Ramey, H.J., Miller, F.G., 1975. Unsteady-state pressure distribution created by a well with an inclined fracture. *Soc. Petr. Eng. SPE-5591* doi:10.2118/5591-MS.
- Cinco-Ley H, Samaniego F, Dominiguez N., 1998. Transient pressure behaviour for a well with a finite-conductivity vertical fracture. *J. Soc. Petr. Eng.*, 253–264.
- Delay F., Kaczmaryk A., Ackerer Ph., 2007. Inversion of interference hydraulic pumping tests in both homogeneous and fractal dual media. *Adv. Wat. Res.*, 30, 314–334. doi:10.1016/j.advwatres.2006.06.008
- Deruyck B., Ehlig-Economides C., Joseph J., 1992. Testing design and analysis. *Oilfield and analysis*. 28-45.
- Dewandel B., Lachassagne P., Zaidi F.K., Chandra S. 2011. A conceptual hydrodynamic model of a geological discontinuity in hard rock aquifers: Example of a quartz reef in granitic terrain in South India. *J. of Hydrol.*, 405, 474-487.
- Dewandel, B., Aunay, B., Maréchal, J.C., Roques, C., Bour, O., Mougin, B., L. Aquilina, 2014. Analytical solutions for analysing pumping tests in a sub-vertical and anisotropic fault zone draining shallow aquifers. *J. of Hydrol.* 509, 115–131.

- 454 Dewandel, B., Alazard, M., Lachassagne, P., Bailly-Comte, V., Couëffé, R., Grataloup, S.,
455 Ladouche, B., Lanini, S., Maréchal, J.C., Wyns, R., 2017. Respective roles of the weathering
456 profile and the tectonic fractures in the structure and functioning of crystalline thermo-mineral
457 carbo-gaseous aquifers. *J. of Hydrol.* 547, 690–707.
- 458 Gringarten, A.C., Ramey, H.J. 1973. The use of Source and Green's functions in solving
459 unsteady-flow problems in reservoirs. *J. Soc. Petr. Eng.* 13, 285-296. SPE-3818-PA.
460 <http://dx.doi.org/10.2118/3818-PA>
- 461 Gringarten, A.C., Ramey, H.J., 1974. Unsteady pressure distribution created by a well with a
462 single horizontal fracture, partial penetration and restricted entry. *J. Soc. Petr. Eng.* 14, 413–
463 426.
- 464 Gringarten, A.C., Henry, J., Ramey, H.J., Raghavan, R., 1974. Unsteady state pressure
465 distributions created by a well with a single infinite conductivity vertical fracture. *J. Soc. Petr.*
466 *Eng.* 14, 347–360.
- 467 Hamm, S.Y., and Bidaux, P., 1996. Dual-porosity fractal models for transient flow analysis in
468 fissured rocks. *Water Resources Research*, 32: 2,733-2,745.
- 469 Hantush, M.S., 1961. Aquifer tests on partially penetrating wells. *Proc. Am. Soc. Civil*
470 *Engin.*, 87, 171-195.
- 471 Hunt, B., 2005. Flow to vertical and nonvertical wells in leaky aquifers. *J. Hydrol. Eng.*,
472 [doi.org/10.1061/\(ASCE\)1084-0699\(2005\)](https://doi.org/10.1061/(ASCE)1084-0699(2005)), vol.10, 477-484.
- 473 Hunt, B., Scott, D., 2007. Flow to a well in a two-aquifer system. *J. Hydrol. Eng.*,
474 [doi.org/10.1061/\(ASCE\)1084-0699\(2007\)](https://doi.org/10.1061/(ASCE)1084-0699(2007)), vol. 12, 146–155.
- 475 Jourde, H., Cornaton, F., Pistre, S., Bidaux, P., 2002. Flow behavior in a dual fracture
476 network. *J. of Hydrol.*, 266, 99-119.
- 477 Lachassagne, P., Wyns, R., Dewandel, B., 2011. The fracture permeability of hard rock
478 aquifers is due neither to tectonics, nor to unloading, but to weathering processes. *Terra Nova*,
479 23, 145-161
- 480 Lashgari, H.R., El Rabaa, W., Chan, H., Vaidya, R., 2014. Estimation of hydraulic fracture
481 contribution in medium to high permeability reservoirs. *Soc. of Petr. Eng.*, n°169554-MS.

- 482 Lolon, E.P., Archer, R.A., Ilk, D., Blasingame, T.A., 2008. New semi-analytical solutions for
483 multilayer reservoirs. Soc. of Petr. Eng., n°114946.
- 484 Maréchal J.C., Dewandel, B., Subrahmanyam K., 2004. Contribution of hydraulic tests at
485 different scale to the characterisation of fracture network properties in hard-rock aquifers.
486 Water Resour. Res., 40 (W11508), 1-17
- 487 Maréchal, J.C., Lachassagne, P., Ladouche, B., Dewandel, B., Lanini, S., Le Strat, P., Petelet-
488 Giraud, E., 2014. Structure and hydrogeochemical functioning of a sparkling natural mineral
489 water system determined using a multidisciplinary approach: a case study from southern
490 France. Hydrogeol. J., 22, 47–68, DOI 10.1007/s10040-013-1073-1
- 491 Newman, A.B. 1936. Heating and cooling rectangular and cylindrical solids. Ind. Eng. Chem.
492 28, 545–548. <http://dx.doi.org/10.1021/ie50317a010>.
- 493 Moench, A.F., 1984. Double-porosity models for a fissured groundwater reservoir with
494 fracture skin, Water Resour. Res., 20, 831-846.
- 495 Muskat, M., 1937. The Flow of Homogeneous Fluids through Porous Media, McGraw-Hill
496 Book Company Inc., New York.
- 497 PetroWiki. Solving unsteady flow problems with Green's and Source functions.
498 <http://petrowiki.org>; SPE International.
- 499 Rafini, S., Larocque M., 2012. Numerical modeling of the hydraulic signatures of horizontal
500 and inclined faults. Hydrogeol. J., 20, 337–350.
- 501 Rafini, S., Chesnaux, R., Ferroud, A., 2017. A numerical investigation of pumping-test
502 responses from contiguous aquifers. Hydrogeol J (2017) 25:877–894. DOI 10.1007/s10040-
503 017-1560-x.
- 504 Renard, Ph., Glenz, D., Mejias, M., 2009. Understanding diagnostic plots for well-test
505 interpretation. Hydrogeol. J., 17, 589–600.
- 506 Roques, C., Bour, O., Aquilina, L., Dewandel, B., 2016. High-yielding aquifers in crystalline
507 basement: insights about the role of fault zones, exemplified by Armorican Massif, France.
508 Hydrogeol. J.. DOI 10.1007/s10040-016-1451-6.

- 509 Russell, D.G., Truitt, N.E., 1964. Transient pressure behavior in vertically fractured
510 reservoirs, J. Pet. Tech. 1159-1170; Trans., AIME, Vol. 231.
- 511 Strelsova, T.D., 1988. Well Testing in Heterogeneous Formations. Exxon Monograph, Ed.
512 John Wiley & Sons, Inc., 413 p.
- 513 Taylor, R., Howard, K., 2000. A tectono-geomorphic model of the hydrogeology of deeply
514 weathered crystalline rock: Evidence from Uganda. Hydrogeol. J., 8, 279-294.
- 515 Theis, C.V., 1935. The relation between the lowering of the piezometric surface and the rate
516 and duration of discharge of a well using groundwater storage. Trans. Am. Geoph. Union, 16,
517 519-524.
- 518 Tiab, D., 2005. Analysis of pressure derivative data of hydraulically fractured wells by the
519 Tiab's Direct Synthesis technique. J. of Petrol. Sci. and Eng., 49, 1–21.
- 520 Thiéry, D., 1980. Analysis of a pumping test in a horizontal fracture. Thomas W Doe. Third
521 Invitational Well-Testing Symposium - well testing in low permeability environments, 26-28,
522 1980, March 1980, Berkeley (California), United States.
- 523 Warren, J.E., P.J. Root, 1963. The behaviour of naturally fractured reservoirs, J. Soc. Petrol.
524 Eng., 3, 245-255.
- 525

Figure captions

Figure 1. Conceptual sketch of a well intercepting a single vertical fracture; it corresponds to the analytical solution of Gringarten et al. (1974) (plan view).

Figure 2. A single fully penetrating fracture in a dual-porosity aquifer (dual-porosity conceptual model: Moench, 1984), pumping at the centre of the fracture. Type curves for various λ coefficients ($\lambda = K_m r^2 / (K_f b_m)$). Dimensionless drawdown $-s_D$: plain curves and derivatives $-s_D'$: dotted curves. Circles correspond to the Gringarten et al. (1974) solution. Dual-porosity model parameters: K_f and K_m , fracture and matrix hydraulic conductivity, b_m : block size, r : radial distance from the well, s_f and s_m : fracture and matrix storage, sk_f : fracture skin.

Figure 3. A single partially entering vertical fracture in a multilayer aquifer. Fracture in the deepest layer, and pumping at the centre of the fracture. a) Conceptual model with aquifer parameters (see text for explanation). b) Type curves for various h_f/B ratios. Circles correspond to the Gringarten et al. (1974) analytical solution.

Figure 4. Pumping at the centre of an inclined fracture in a leaky aquifer system. a) Conceptual model with aquifer parameters (see text for explanation). b) Type curves for various angles of the fracture with the vertical, θ , and $k'/B' = 0$ (no-leakage). Dots correspond to the Gringarten et al. (1974) and Thiéry (1980) analytical solutions.

Figure 5. Two inclined fractures in a leaky aquifer system: model parameters.

Figure 6. Two inclined fractures in a leaky aquifer system; the well is screened in front of both fractures only. a) Average drawdown and its derivative at the well. b) Dimensionless flowrate contributions of each fracture. c), d), e) and f) Drawdown distributions at various times along the x-axis. Pumping rate is $1 \text{ m}^3/\text{h}$.

Figure 7. Two inclined fractures in a leaky aquifer system, pumping in the fractures and in the aquifer through a fully penetrating well. a) Average drawdown and its derivative at the well. b) Dimensionless flowrate contributions of each fracture and of the aquifer through the well. c), d), e) and f) Drawdown distributions at various times along the x-axis. Pumping rate is $1 \text{ m}^3/\text{h}$.

Caption for the figure in Appendix C: drawdown and its derivative (a) and flowrates (b) behaviour for a well screened in front of both fractures (length: 7 m); both fractures and the

aquifer though the screened-interval are pumped. Fractures and aquifer properties are the ones of Figure 5. Pumping rate is $1 \text{ m}^3/\text{h}$.

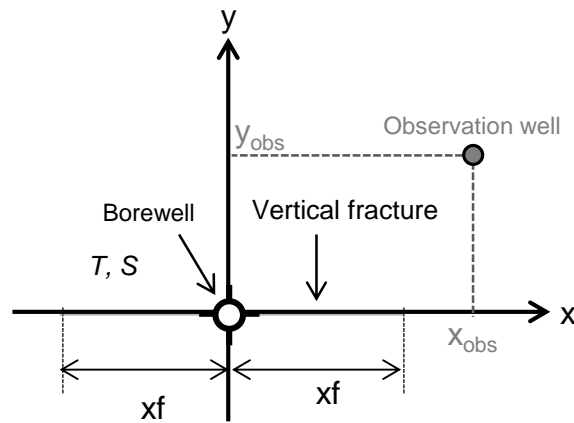


Figure 1. Conceptual sketch of a well intercepting a single vertical fracture; it corresponds to the analytical solution of Gringarten et al. (1974) (plan view).

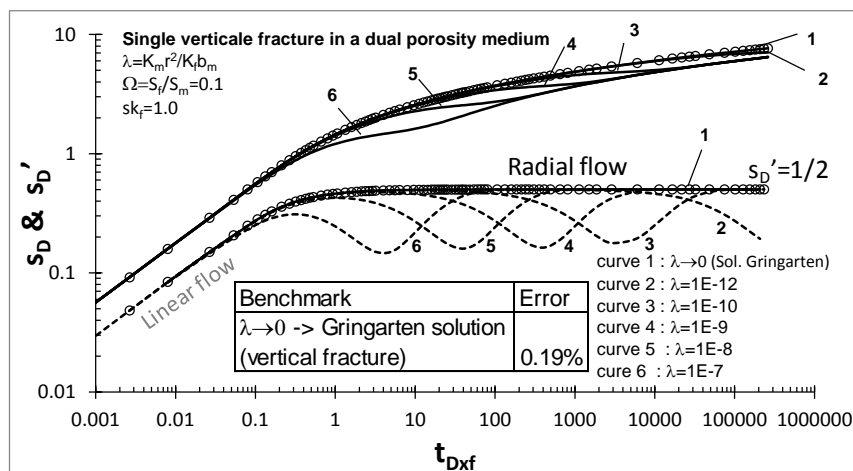
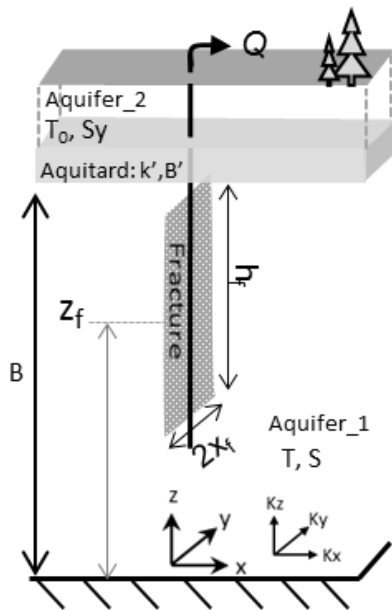
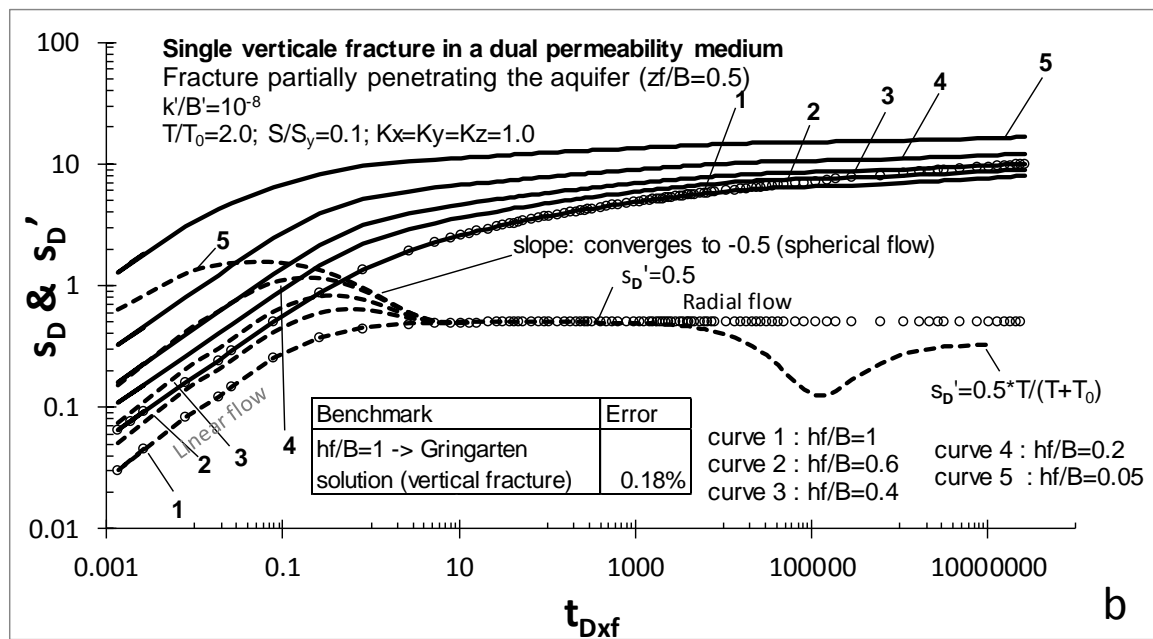


Figure 2. A single fully penetrating fracture in a dual-porosity aquifer (dual-porosity conceptual model: Moench, 1984), pumping at the centre of the fracture. Type curves for various λ coefficients ($\lambda = K_m r^2 / (K_f b_m)$). Drawdown $-s_D$: plain curves and derivatives $-s_D'$: dotted curves. Circles correspond to the Gringarten et al. (1974) solution. Dual-porosity model parameters: K_f and K_m , fracture and matrix hydraulic conductivity, b_m : block size, r : radial distance from the well, s_f and s_m : fracture and matrix storage, sk_f : fracture skin.



a



b

Figure 3. A single partially entering vertical fracture in a multilayer aquifer. Fracture in the deepest layer, and pumping at the centre of the fracture. a) Conceptual model with aquifer parameters (see text for explanation). b) Type curves for various h_f/B ratios. Circles correspond to the Gringarten et al. (1974) analytical solution.

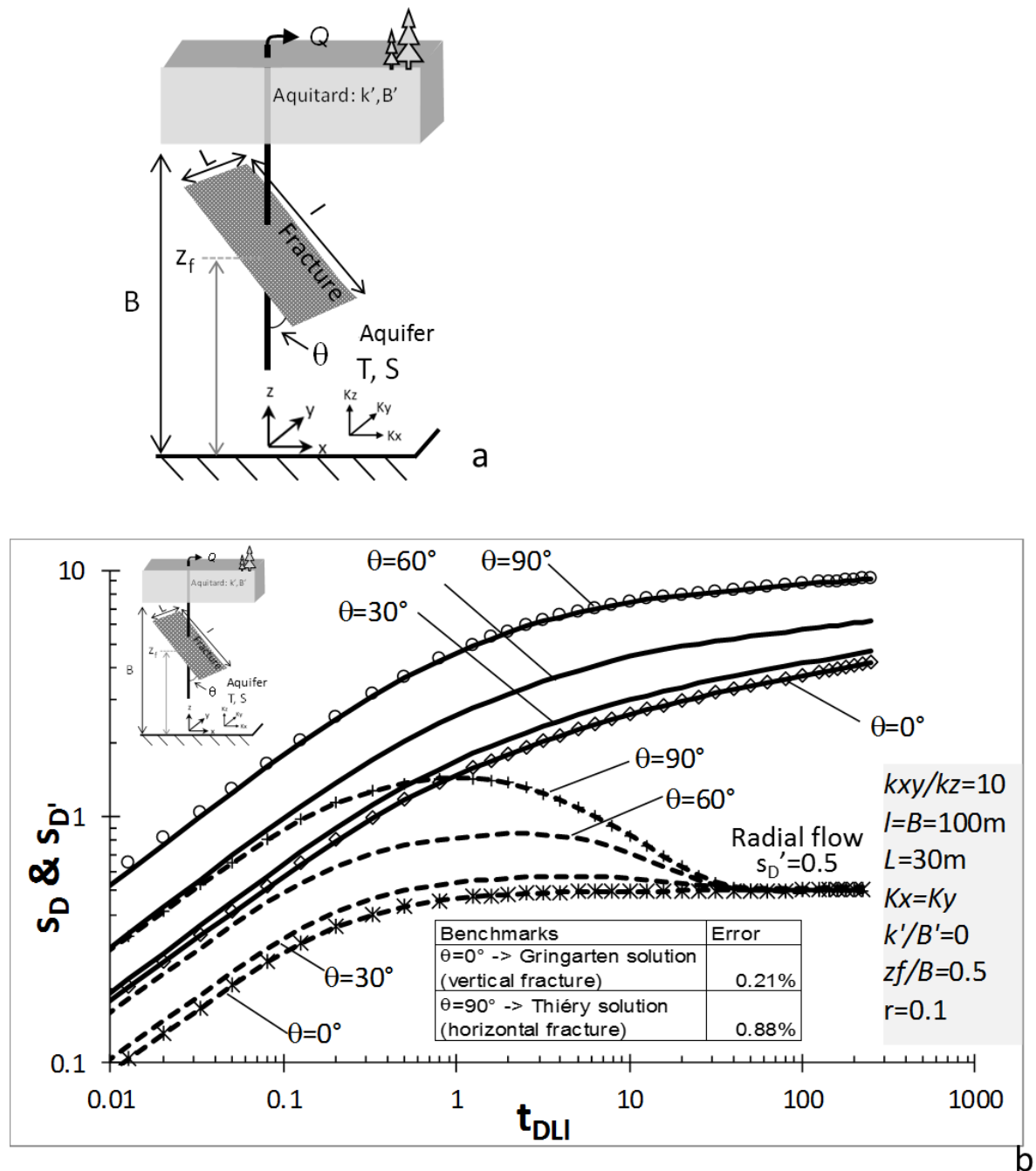


Figure 4. Pumping at the centre of an inclined fracture in a leaky aquifer system. a) Conceptual model with aquifer parameters (see text for explanation). b) Type curves for various angles of the fracture with the vertical, θ , and $k'/B' = 0$ (no-leakage). Dots correspond to the Gringarten et al. (1974) and Thiéry (1980) analytical solutions.

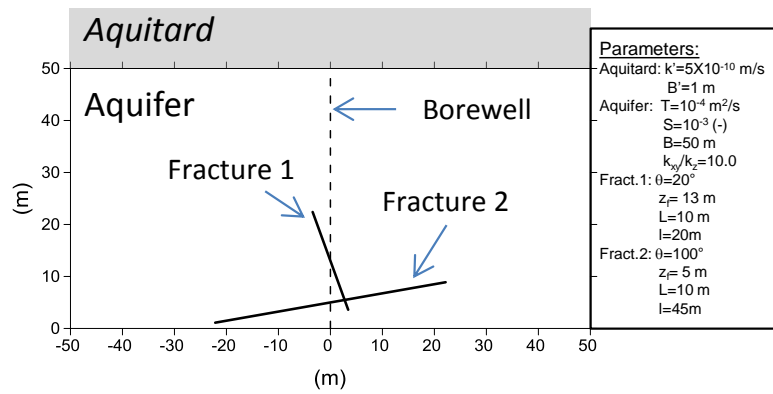


Figure 5. Two inclined fractures in a leaky aquifer system: model parameters.

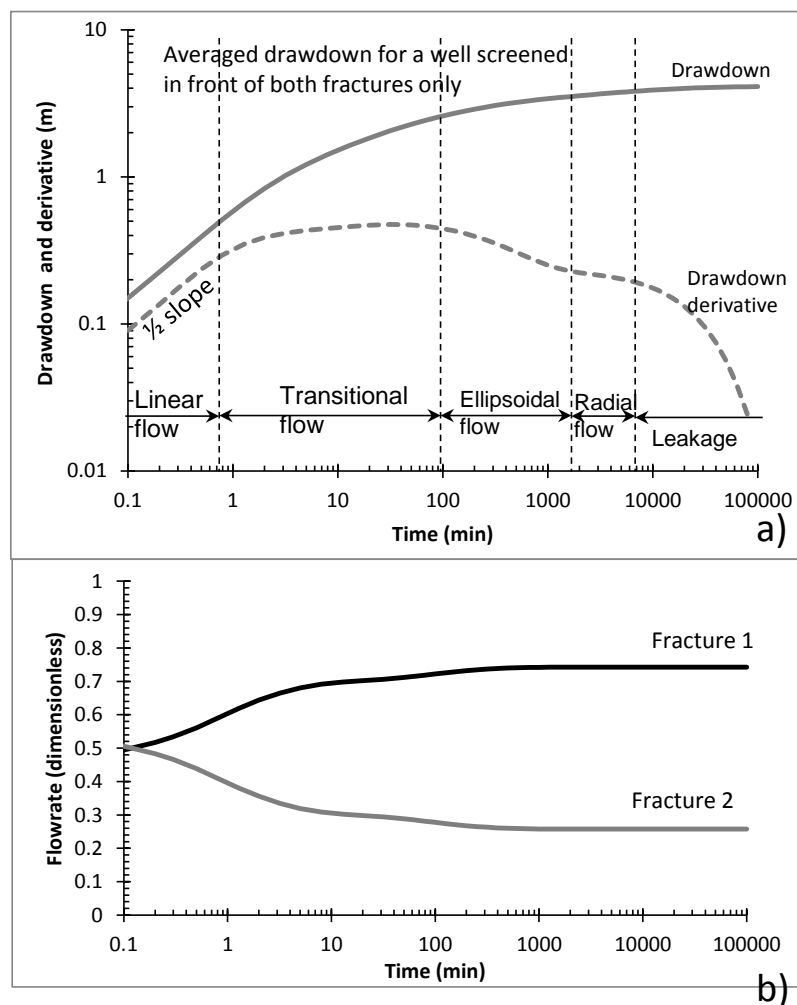


Figure 6. Two inclined fractures in a leaky aquifer system; the well is screened in front of both fractures only. a) Average drawdown and its derivative at the well. b) Dimensionless flowrate contributions of each fracture. Pumping rate is $1 \text{ m}^3/\text{h}$.

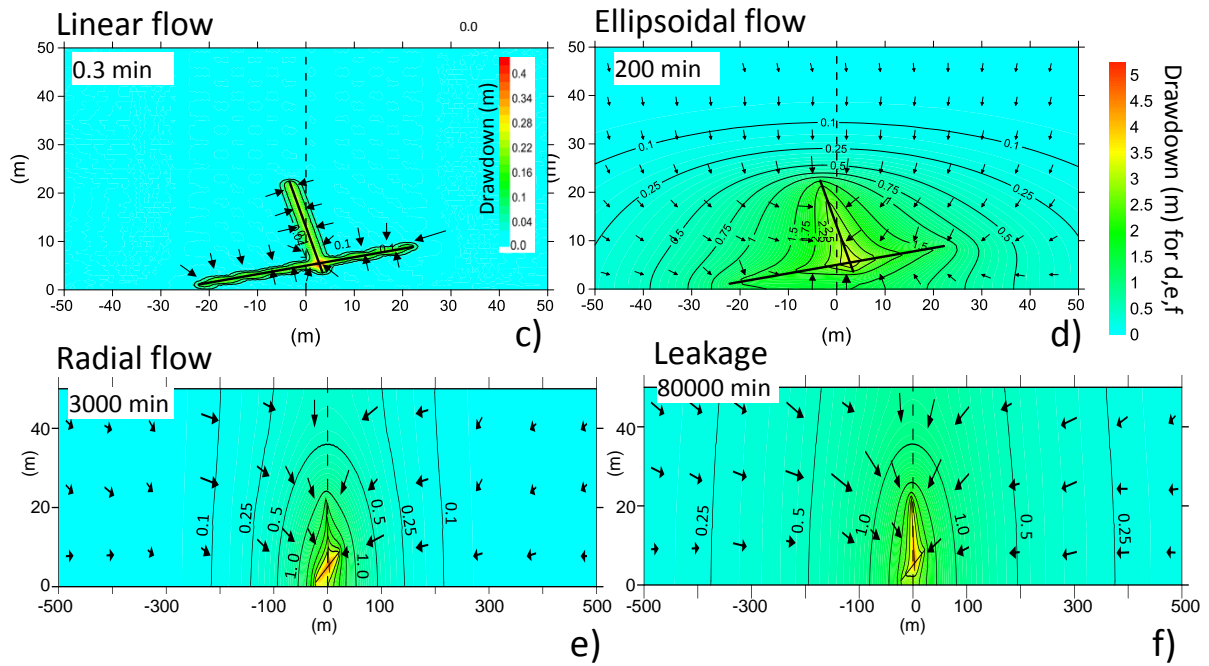


Figure 6. cont'd. c), d), e) and f) Drawdown distributions at various times along the x-axis.

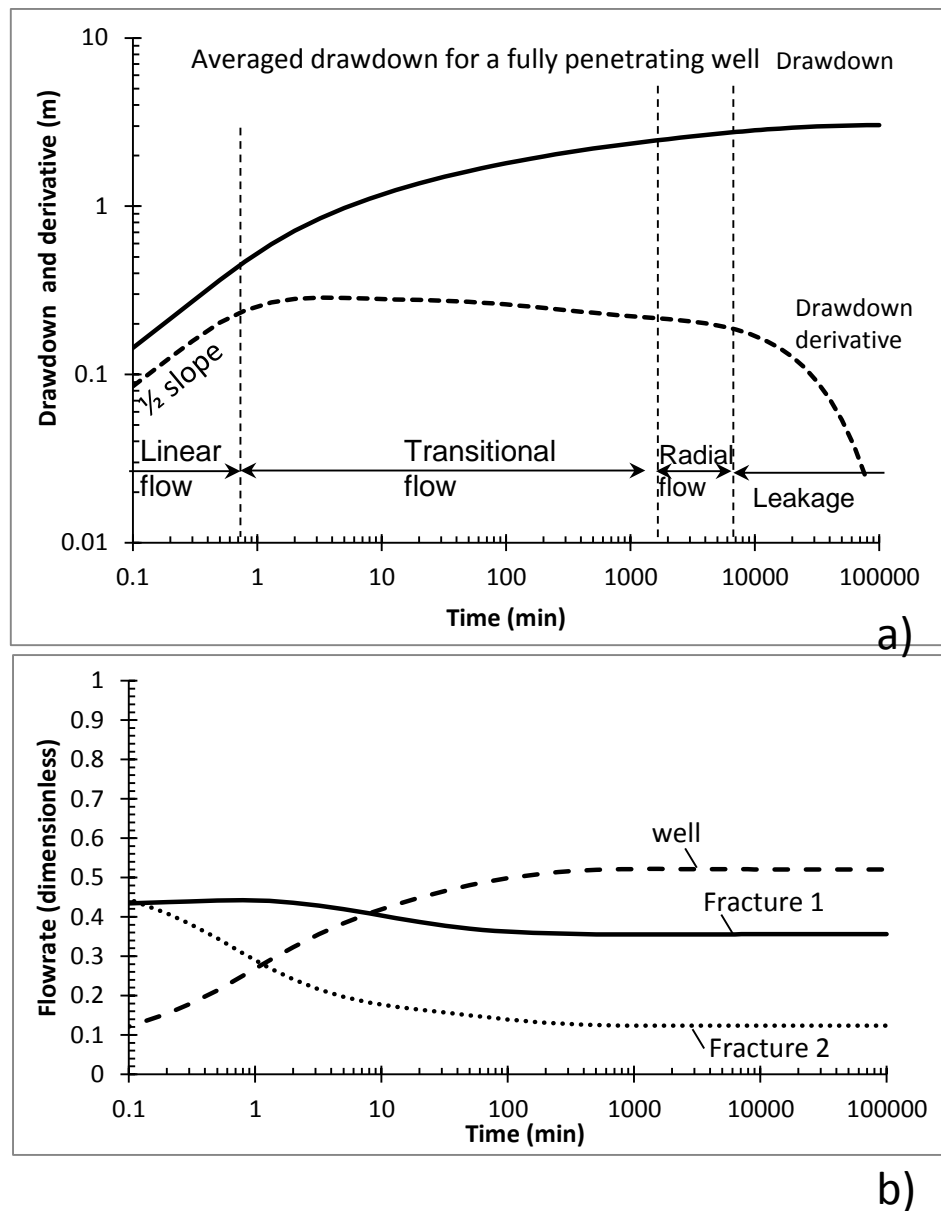


Figure 7. Two inclined fractures in a leaky aquifer system, pumping in the fractures and in the aquifer through a fully penetrating well. a) Average drawdown and its derivative at the well. b) Dimensionless flowrate contributions of each fracture and, of the aquifer through the well. Pumping rate is $1 \text{ m}^3/\text{h}$.

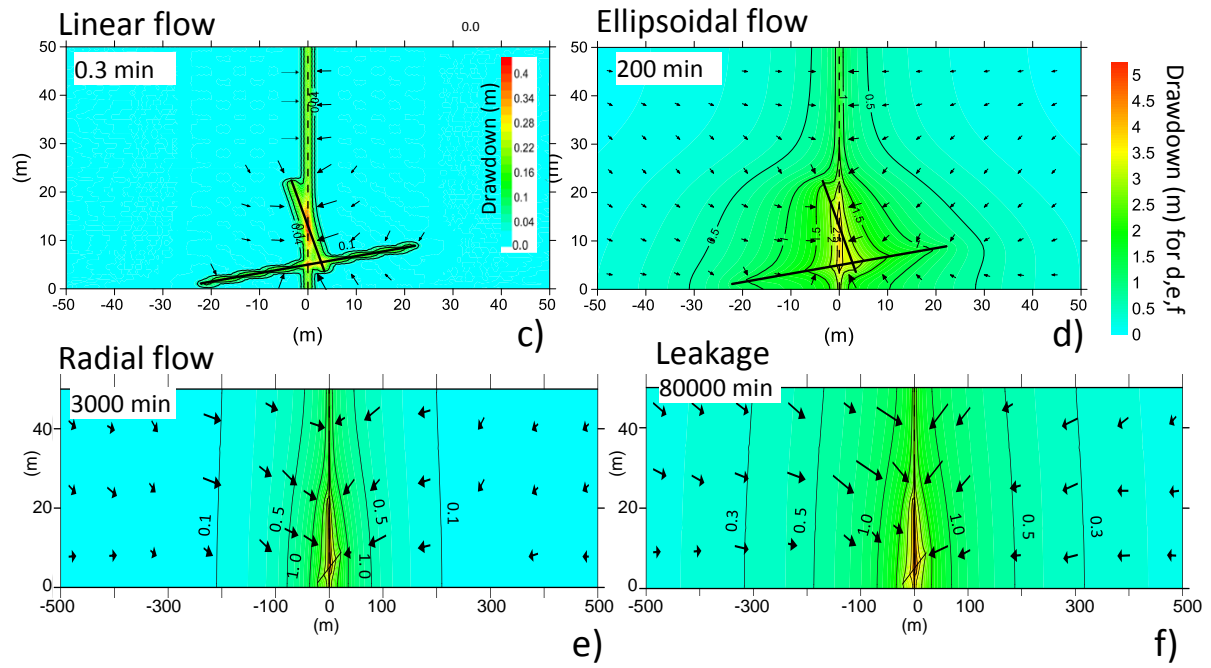


Figure 7. cont'd. c), d), e) and f) Drawdown distributions at various times along the x-axis.

Appendices:

Appendix A: Dimensionless drawdown and time

Dimensionless drawdown, s_D :

$$s_D = \frac{2\pi T}{Q} s$$

With s , the drawdown, T , the transmissivity, and Q , the pumping rate.

Dimensionless time, t_{Dxf} and t_{DLI} :

- For a vertical fracture fully penetrating the aquifer, t_{Dxf} :

$$t_{Dxf} = \frac{tT}{Sx_f^2}; \text{ with } x_f, \text{ the half-fracture length, } t, \text{ the time and } S, \text{ the storage coefficient of the aquifer.}$$

- For a fracture partially penetrating the aquifer, t_{DLI} :

$$t_{DLI} = \frac{tT}{S(L/2.l/2)}; \text{ with } L \text{ and } l, \text{ the length and the width of the fracture.}$$

Appendix B: point-source solution of Hunt (2005)

Point-source (or sink source) solution for the aquifer described in Figure 4 (Hunt, 2005), from which 3-D anisotropy in hydraulic conductivity has been implemented:

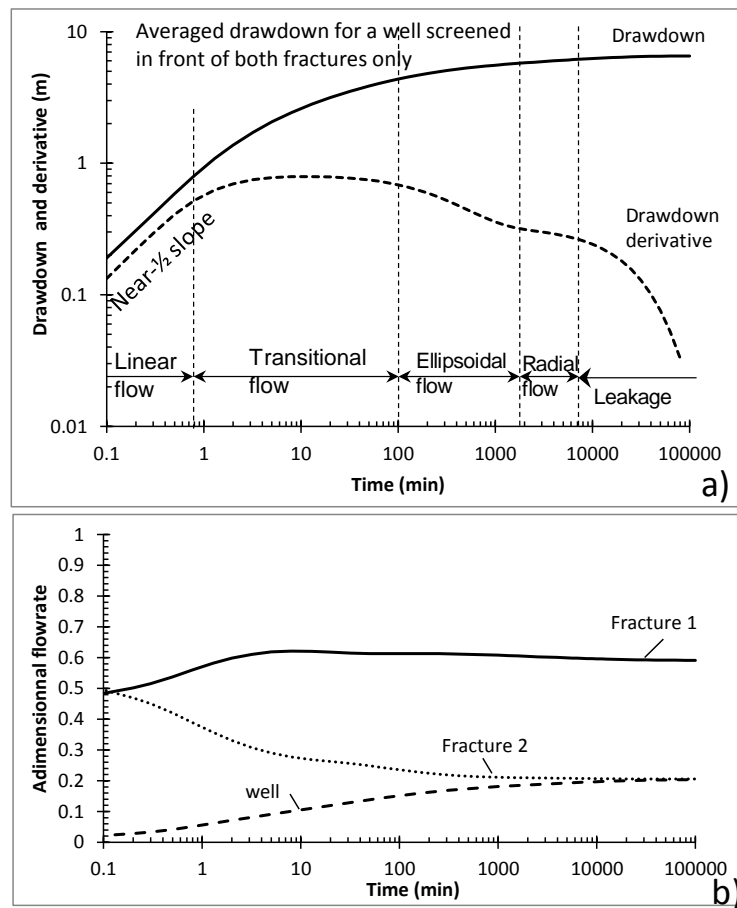
$$s_{\text{sink}}(x_D, y_D, z_D, t_D) = \frac{Q}{2\pi T} \sum_{n=1}^{\infty} \frac{\cos(\alpha_n Z/B) \cos(\alpha_n z_D)}{1 + \frac{\sin(2\alpha_n)}{2\alpha_n}} W\left(\frac{(r/B)^2}{4t_D}, \alpha_n \frac{r}{B} \sqrt{k_z/k_{xy}}\right)$$

where $x_D = \frac{x}{B} \sqrt{k_y/k_{xy}}$, $y_D = \frac{y}{B} \sqrt{k_x/k_{xy}}$, $z_D = \frac{z}{B}$, are dimensionless variables of the point location (x, y, z); k_x, k_y, k_z are the hydraulic conductivity along the x, y, z directions; Z is the z coordinate of the point source where pumping Q takes place; k_{xy} is the horizontal hydraulic conductivity of the aquifer ($k_{xy} = \sqrt{k_x k_y} = T/B$); B is the aquifer thickness and $t_D = tk_{xy}/SB$;

621 t is time; α_n is the root of equation $\alpha_n \tan(\alpha_n) = \frac{k'/B'}{k_z/B}$, with k' and B' the hydraulic
 622 conductivity and the thickness of the leaky aquifer; $W(a, b)$ is the Hantush leaky-aquifer well
 623 function.

624

625 **Appendix C:** drawdown and its derivative (a) and flowrates (b) behaviour for a well screened
 626 in front of both fractures (length: 7 m); both fractures and the aquifer through the screened-
 627 interval are pumped. Fractures and aquifer properties are the ones of Figure 5. Pumping rate is
 628 $1 \text{ m}^3/\text{h}$.



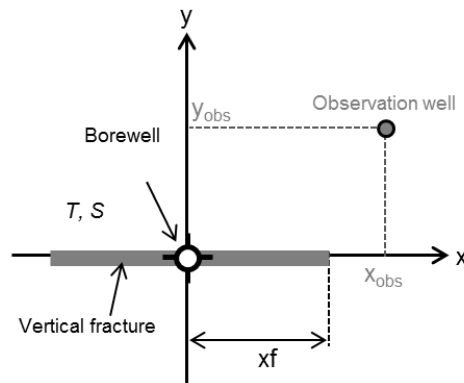
629

630

Supplemental material:

Demonstrating that the well Theis function integrated along a fracture plane is identical to the analytical solution of pumping in a vertical fracture proposed by Gringarten et al. (1974) with uniform flux distribution.

Definition conceptual model: the borewell intercepts a vertical fracture of length $2xf$ in a homogeneous and infinite aquifer of transmissivity, T , and storativity, S . The width of the fracture is assumed to be negligible.

**Notations**

$$r^2 = (x - x_{obs})^2 + y_{obs}^2 \text{ with } x \text{ a point in the fracture ; } t_D = \frac{Tt}{x_f^2 S} ; x_D = \frac{x_{obs}}{x_f} ; y_D = \frac{y_{obs}}{x_f} ;$$

$$u = \frac{r^2 \cdot S}{4Tt} \Rightarrow u = \frac{(x - x_{obs})^2 + y_{obs}^2}{4Tt} S = \frac{(x/x_f - x_D)^2 + y_D^2}{4t_D} \text{ and } a = u \cdot t_D = \frac{(x/x_f - x_D)^2 + y_D^2}{4}$$

Properties of the well function $W(u)$:

$$W(u) = E_1(u) = -E_i(-u) = \int_u^\infty \frac{e^{-y}}{y} dy$$

$$\text{With the following change of variable: } y = \frac{a}{\tau}, \text{ it becomes that } \int_{a/t_D}^\infty \frac{e^{-y}}{y} dy = \int_0^{t_D} \frac{e^{-a/\tau}}{\tau} d\tau$$

Properties of the Erf function:

$$Erf(x) = \frac{2}{\sqrt{\pi}} \int_0^x e^{-u^2} du = -\frac{2}{\sqrt{\pi}} \int_{-x}^0 e^{-u^2} du$$

$$Erf(x) = -Erf(-x)$$

Well Theis function for a well

The aquifer is pumped in a single vertical well fully penetrating the aquifer with a pumping rate q . The drawdown at a radial distance r from the well can be expressed as:

$$\begin{cases} s(r, t) = \frac{q}{4\pi T} W(u) = \frac{q}{4\pi T} \int_u^\infty \frac{e^{-y}}{y} dy \\ u = \frac{r^2 S}{4Tt} \end{cases} \quad [\text{Eq.1}]$$

Gringarten analytical solution (Gringarten et al., 1974)

For a pumping in a single vertical fracture intersecting the pumped well, with uniform flux distribution, the drawdown can be expressed as:

$$s(x, y, t) = \frac{Q}{2\pi T} s_D \quad \text{with} \quad s_D = \int_0^{t_D} e^{-\frac{y_D^2}{4\tau}} \left[\text{Erf}\left(\frac{1-x_D}{2\sqrt{\tau}}\right) - \text{Erf}\left(\frac{1+x_D}{2\sqrt{\tau}}\right) \right] \frac{\sqrt{\pi}}{4\sqrt{\tau}} d\tau \quad [\text{Eq.2}]$$

Where Q is the pumping rate. As Q is assumed to be uniformly distributed along the fracture, therefore:

$$Q = \int_{-x_f}^{+x_f} q(x) dx \Rightarrow q(x) = q = \frac{Q}{2x_f}$$

Mathematical demonstration

Integration of the Theis' solution along the fracture yields:

$$s_I(x, y, t) = \int_{-x_f}^{+x_f} s(x, y, t) dx = \frac{1}{4\pi T} \int_{-x_f}^{+x_f} q E_1\left(\frac{(x-x_{obs})^2 + y_{obs}^2}{4Tt}\right) S dx$$

with the simplified notation and using the property of the E_1 function, it becomes:

$$s_I = \frac{Q}{2\pi T} \frac{1}{4x_f} \int_{-x_f}^{+x_f} E_1\left(\frac{a}{t_D}\right) dx = \frac{Q}{2\pi T} \frac{1}{4x_f} \int_{-x_f}^{+x_f} \left(\int_{a/t_D}^{+\infty} \frac{e^{-u}}{u} du \right) dx = \frac{Q}{2\pi T} \frac{1}{4x_f} \int_{-x_f}^{+x_f} \left(\int_0^{t_D} \frac{e^{-a/\tau}}{\tau} d\tau \right) dx$$

$$\text{which can be rewritten as : } s_I = \frac{Q}{2\pi T} \frac{1}{4x_f} \int_{-x_f}^{+x_f} \left(\int_0^{t_D} \frac{e^{-\left[\left(\frac{x}{x_f} - x_D\right)^2 + y_D^2\right]/4\tau}}{\tau} d\tau \right) dx$$

According to the Fubini theorem (i.e. τ and x are independent), the order of integration can be inverted, yielding to:

$$s_I = \frac{Q}{2\pi T} \frac{1}{x_f} \int_{-x_f}^{+x_f} \left(\int_0^{t_D} e^{-y_D^2/4\tau} \frac{e^{-\left(\frac{x}{x_f} - x_D\right)^2/4\tau}}{4\tau} d\tau \right) dx = \frac{Q}{2\pi T} \frac{1}{x_f} \int_0^{t_D} \left(\int_{-x_f}^{+x_f} e^{-y_D^2/4\tau} \frac{e^{-\left(\frac{x}{x_f} - x_D\right)^2/4\tau}}{4\tau} dx \right) d\tau$$

and as $e^{-y_D^2/4\tau}$ does not depend on x , it can be rearranged as:

$$s_I = \frac{Q}{2\pi T} \frac{1}{x_f} \int_0^{t_D} e^{-y_D^2/4\tau} \underbrace{\left(\int_{-x_f}^{+x_f} \frac{e^{-\left(\frac{x}{x_f} - x_D\right)^2/4\tau}}{4\tau} dx \right)}_{(a)} d\tau \quad [\text{Eq.3}]$$

With the following change of variable: $v = \left(\frac{x}{x_f} - x_D\right)/2\sqrt{\tau}$, the (a) term of [Eq.3] can be rewritten as :

$$\int_{-x_f}^{+x_f} \frac{e^{-\left(\frac{x}{x_f} - x_D\right)^2/4\tau}}{4\tau} dx = \frac{x_f}{4\sqrt{\tau}} \int_{-(1+x_D)/2\sqrt{\tau}}^{(1-x_D)/2\sqrt{\tau}} 2e^{-v^2} dv \quad [\text{Eq.4}]$$

The right part of [Eq.4] can be decomposed into two terms related to the *Erf* function:

$$\frac{x_f}{4\sqrt{\tau}} \int_{-(1+x_D)/2\sqrt{\tau}}^{(1-x_D)/2\sqrt{\tau}} 2e^{-v^2} dv = \frac{x_f}{4\sqrt{\tau}} \left(\int_{-(1+x_D)/2\sqrt{\tau}}^0 2e^{-v^2} dv + \int_0^{(1-x_D)/2\sqrt{\tau}} 2e^{-v^2} dv \right) = \frac{x_f \cdot \sqrt{\pi}}{4\sqrt{\tau}} \left[-\text{Erf}\left(\frac{(1+x_D)}{2\sqrt{\tau}}\right) + \text{Erf}\left(\frac{(1-x_D)}{2\sqrt{\tau}}\right) \right] \quad [\text{Eq.5}]$$

Combining [Eq.3] and [Eq.5], we obtain:

$$s_I = \frac{Q}{2\pi T} \frac{1}{x_f} \int_0^{t_D} e^{-\frac{y_D^2}{4\tau}} \frac{x_f \sqrt{\pi}}{4\sqrt{\tau}} \left[-\text{Erf}\left(\frac{(1+x_D)}{2\sqrt{\tau}}\right) + \text{Erf}\left(\frac{(1-x_D)}{2\sqrt{\tau}}\right) \right] d\tau$$

$$\text{And thus : } s_I = \frac{Q}{2\pi T} \int_0^{t_D} e^{-\frac{y_D^2}{4\tau}} \left[\text{Erf}\left(\frac{(1-x_D)}{2\sqrt{\tau}}\right) - \text{Erf}\left(\frac{(1+x_D)}{2\sqrt{\tau}}\right) \right] \frac{\sqrt{\pi}}{4\sqrt{\tau}} d\tau \quad [\text{Eq.6}]$$

[Eq.6] proves that the Theis analytical solution integrated along the fracture plane is exactly the same as the Gringarten analytical solution, for a vertical fracture with a uniform flux distribution (Eq. 2 or the Eq. 20 in Gringarten et al. 1974).

